Title: Selective HDS of DBT using a K_2O-modified CoMoW/Al_2O_3-MgO catalytic formulation

Authors: D.A. Solís-Casados, C.E. Rodríguez-Nava, T. Klimova, L. Escobar-Alarcón

PII: S0920-5861(19)30389-X
DOI: https://doi.org/10.1016/j.cattod.2019.07.029
Reference: CATTOD 12358

To appear in: *Catalysis Today*

Received date: 22 April 2019
Revised date: 2 July 2019
Accepted date: 20 July 2019

Please cite this article as: Solís-Casados DA, Rodríguez-Nava CE, Klimova T, Escobar-Alarcón L, Selective HDS of DBT using a K_2O-modified CoMoW/Al_2O_3-MgO catalytic formulation, *Catalysis Today* (2019), https://doi.org/10.1016/j.cattod.2019.07.029

Selective HDS of DBT using a K_2O-modified CoMoW/Al_2O_3-MgO catalytic formulation

D. A. Solís-Casados[*, 1], C. E. Rodríguez-Nava[1,2], T. Klimova[3], L. Escobar-Alarcón[4]

[1]*Universidad Autónoma del Estado de México. Facultad de Química, Centro Conjunto de Investigación en Química Sustentable UAEM-UNAM. Carretera Toluca-Atlacomulco km. 14.5, San Cayetano, Toluca, Méx.*

[2]*Maestría en Ciencia de Materiales de la Facultad de Química, Universidad Autónoma del Estado de México, Paseo Colón Esquina Paseo Tollocan S/N, Toluca Estado de México, México, C.P. 50000.*

[3]*Universidad Nacional Autónoma de México. Circuito Exterior S/N, Coyoacán, Cd. Universitaria, Ciudad de México,*

[4]*Instituto Nacional de Investigaciones Nucleares, Carretera México-Toluca km 36.5, Ocoyoacac, Méx.*

*solis_casados@yahoo.com.mx

Graphical Abstract

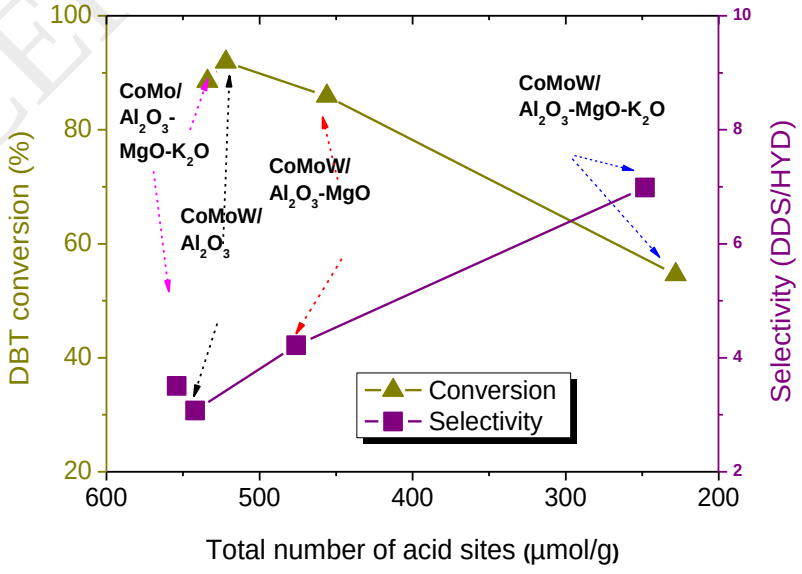

Highligths

- Novel catalytic formulation with good selectivity towards direct desulfurization was obtained.
- The addition of magnesia and potash to the catalytic support decreases the number of acid sites
- Low hydrogenating function increases selectivity toward BP products.

Abstract:

Novel catalytic formulation CoMoW/Al2O3-MgO-K2O with low acidity and good selectivity towards direct desulfurization was obtained.It is observed that the addition of magnesia and potash to the catalytic support decreases the total number of acid sites determined through TPD of NH3. Supports were impregnated with a solution containing the metallic precursors of CoMoW as the respective citrates. From images obtained by TEM was made the statistical analyses of the stacking and slab length of MoS2 and WS2 crystallites, it was observed slabs larger and more stacked for the catalytic formulation containing K2O; their catalytic activity was evaluated through HDS of DBT to investigate their catalytic performance, and products such as BP, DCH and CHB were quantified to obtain selectivity through ratio of BP/CHB+DCH. Even when the catalytic formulation with low acidity shows a good selectivity the global activitydecreases.

Keywords: selective desulphurization, dibenzothiophene, CoMoW catalysts, low acidity formulations

1. Introduction

In the last twenty years conventional catalytic formulation as Co or Ni (Mo or W) to remove sulfur in fuels have been studied. The main purpose has been to decrease SOx emission from internal combustion engines, machines and automotive vehicles to preserve the environment [1-4]. This to comply with regulations imposed for the government and the organizations involved with air pollution control. One of the important challenges that the researchers found is when sulfur is eliminated from the molecules that make up the fuels, the unsaturated molecules are hydrogenated, which is undesirable since the olefinic unsaturated molecules

provide the octane number in the fuels [5-10]. This is the reason why it is important to understand how to modify the catalytic formulations to carry out the sulfur removal of fuels selectively. Sulphur elimination from the molecules that compose the fuels by the hydrodesulphurization (HDS) process causes hydrogenation of the olefinic unsaturated molecules leading to a decrease in the octane number in the fuels [5-10]. To address this issue, it is very important to investigate selective catalytic formulations able to remove sulphur efficiently with the hydrogenation as low as possible and consequently keeping the octane number in the fuels.

Traditionally, conventional catalytic formulations of CoMo or NiMo supported on γ-Al_2O_3 for sulphur remotion from molecules of the petroleum refining processes have been investigated [11-13]. Their catalytic behavior has been studied using DBT and/or 4,6 DMDBT molecules as the most commonly employed [14-18]. The reported results show that these conventional catalytic formulations have the disadvantage of hydrogenate some reaction products such as biphenyl resulting ciclohexylbenzene and diciclohexyl which decrease the unsaturated products [19-21].

To improve the catalytic performance towards selective desulphurization, the use of low acidity formulations has been proposed. Particularly, the addition to the catalytic support of some oxides containing basic sites, such as lithia, magnesia, potash, lanthana and in some cases ceria has given good results enhancing selectivity towards byphenyl-type compounds in the hydrodesulphurization (HDS) of dibenzothiophene (DBT) [22-24]. However, even when the low acidity formulations show a good catalytic selectivity the global activity decreases slightly [25]. With the purpose of overcome this issue the addition of another active site, such as WS_2, to obtain a trimetallic catalytic formulation (CoMoW) on a low acidity support has been studied [26]. In this line, it is reported in this work the preparation of CoMoW trimetallic catalytic formulations with low acidity. The prepared impregnating solution CoMoW was stabilized with citric acid as a chelant agent, to obtain good dispersion of the precursors of the active phases [27]. This impregnating solution was deposited on a low acidity Al_2O_3-MgO-K_2O support, as well as on Al_2O_3-MgO and Al_2O_3 supports which were used as references.

2. Experimental Procedure

2.1. Supports

A paste of aluminium hydroxide was prepared from 11.8 g of pseudo-Boehmite Catapal B TM Sassol (AlOOH) in powder, which was formed using 5.2 mL of formic acid (HCOOH

sigma, ACS reagent ≥ 96%) 5 % vol and 4.6 mL of distilled water. This paste was extruded using a syringe to produce pellets which were dried overnight under environmental conditions and thermally treated at 100 ^{o}C for 2 h and afterwards at 400 ^{o}C for 4 h, using a heating rate of 5 ^{o}C/min in an air convection oven. Thermal treatment was used to eliminate the formic acid and to reach the complete dehydroxylation to obtain alumina in its gamma crystalline phase.

The precursor paste used to obtain the pellets of the Al_2O_3-MgO support was prepared mixing 11.2 g of pseudo-Boehmite Catapal B with 1.4 g of magnesium ethoxide ($Mg(OC_2H_5)_2$) ACS reagent from Aldrich to get a nominal composition of 5 wt. % of MgO in the Al_2O_3-MgO support; 6 mL formic acid (HCOOH) 5 % vol and 6 mL of distilled water were used. This jellified mixture was extruded to get the Al_2O_3-MgO support in its pelletized form. These pellets were thermally treated in the same way than the Al_2O_3 pellets. To obtain the Al_2O_3-MgO-K_2O support, 4 g of Al_2O_3-MgO support were impregnated with an aqueous KOH solution (0.09 g KOH/mL) by the incipient wetness technique to get 5 wt. % of K_2O, supports were aged under environmental conditions for 12 h to equilibrate solids; afterwards, were subjected to the thermal treatment described previously.

2.2. Precursors of CoMoW catalysts

To obtain the precursors of CoMoW catalysts, firstly was prepared a low acidity solution (6 NH_4OH:1 H_2O) containing ions of these metals; to prepare this solution were added 3 g of molybdenum trioxide (MoO_3, Fermont), 1.9 g of monohydrated cobalt carbonate ($CoCO_3$ H_2O, Aldrich, 99.98% trace metal basis), 2.4 g of ammonium metatungstate ($(NH_4)_6H_2W_{12}O_{40}$ H_2O), Aldrich, ≥ 85%). The final solution was obtained using 12 g of citric acid ($HOC(COOH)(CH_2COOH)_2$, Aldrich, ≥ 99.5%) as a chelating agent, after impregnation it is expected to get a high metallic atomic charge dispersed onto the support with approximated theoretical ratios of [Co/(Co+Mo)] = 0.4 and [W/(Co+W)] = 0.4. The obtained CoMoW solution was impregnated by the incipient wetness technique on the three supports:Al_2O_3, Al_2O_3-MgO and Al_2O_3-MgO-K_2O, the impregnated pellets were aged during 12 h under environmental conditions to reach the impregnation equilibrium; after that, they were thermally treated at 400 ^{o}C for 4 h at a heating rate of 5 ^{o}C/min.

2.3. Characterization of supports, catalytic precursors and catalysts

Supports and precursors of catalysts in their oxidic form were characterized through several characterization techniques such as thermal analysis, N_2 physisorption, X-ray powder diffraction (XRD), Infrared (IR), UV-Vis DRS, X-ray photoelectron (XPS) and Raman spectroscopies, temperature-programmed reduction (TPR) and ammonia thermodesorption (NH_3-TPD). Sulfided catalyst were characterized through transmission electron microscopy (TEM).

2.3.1 Thermal analysis

Thermogravimetric analysis (TGA) and differential scanning calorimetry (DSC) were done in pellets of the Al_2O_3, Al_2O_3-MgO and Al_2O_3-MgO-K_2O supports previously to the thermal treatment, to determine the suitable temperature of thermal treatment to obtain the oxidized supports. Analysis was performed in a SDT Q600 Thermo Gravimetric Analyzer under an oxygen flow (10 mL / min) from room temperature up to 1000 ºC with a heating rate of 10 ºC / min, whereas the weight loss and heat flow in the sample were followed. Weight loss indicates water elimination and removal of some organic compounds present in the samples and when the weight remains constant the complete dihydroxylation of samples is reached. The heat flow indicates dehydroxylation and crystallization process in samples through an exothermic peak.

2.3.2 N_2 physisorption

Textural properties such as specific surface area, pore volume and pore diameter distribution were determined through N_2 physisorption technique in supports and catalysts precursors using a 3-flex equipment from Micromeritics. Adsorption isotherms were analyzed accordingly to the International Union of Pure and Applied Chemistry (IUPAC) rules to estimate pore sizes and hysteresis cycle was used to elucidate the form of the pore [28]. Supports and catalysts precursors were characterized through this technique, determining their specific surface area through the multipoint theory using the Brunauer-Emmet-Teller equation (BET). The kelvin equation was employed to determine the pore size whereas the pore size distribution was determined through the Barrett-Joyner-Halenda (BJH) equation. The total pore volume was measured at relative pressure (P/P◦) equal to 0.98.

Supports were previously degassed out at 250 ºC during 5 h (P $<10^{-1}$ Pa) and catalytic precursors were degassed out at 270 ºC during 10 h to evacuate physisorbed water and gases

such as the CO_2 from the inner of porous, previously to the N_2-physisorption analysis. The experimental error of this technique is close to 3% (≅ $7m^2/g$).

2.3.3 X-Ray powder diffraction

Crystalline phases identification was done using X-ray powder diffraction (XRD), which was carried out in a Bruker D8 Advance diffractometer, equipped with a Linxeye detector, using Cu Kα radiation Ni-filtered to identify crystalline phases in supports and catalysts precursors. The analysis conditions were: 2θ = 20–80°, step = 0.021° and acquisition time = 2.5 s per step.

2.3.4 Infrared spectroscopy

Infrared spectroscopy (IR) was used to corroborate the elimination of organic compounds and to study some functional groups such as the carbonate ones. IR spectra were obtained with a Bruker infrared equipment, model Tensor 27 with Platinum ATR accessory, analyzing the samples from 4000 to 400 cm^{-1}, 4 cm^{-1} resolution and 32 scans.

2.3.5 UV-Vis DRS spectroscopy

From UV–Vis DRS spectra were determined chemical coordination state and electronic transitions. The spectra were recorded in a wavelength range from 190 to 1100 nm with a slit of 1nm using a lambda-35 spectrophotometer from Perkin Elmer equipped with a diffuse reflectance (DRS) sphere. Band gap energy was determined through the Kubelka Munk function from the DRS spectra. As was reported by Weber before [29], the band gap energy values can be related following an empirical procedure with the particle aggregation through the near neighbor's correlations, if average sizes of the molybdenum oxide, tungsten oxide and cobalt oxide domains increase as the metal loading increases.

2.3.6 X-ray photoelectron spectroscopy

Supports and catalysts precursors were characterized by X-ray photoelectron spectroscopy (XPS) mainly to determine the elemental chemical composition on catalytic surface. A JEOL JPS 9200 XPS equipment was employed to determine the elemental content in each sample and their oxidation state. Wide and narrow spectra were acquired using an Al Kα X-ray source. Charge correction was done adjusting the C1s to 285 eV to analyze the chemical environment of each element.

2.3.7 Raman spectroscopy

Microstructural characteristics of the supports and catalysts were studied by MicroRaman Spectroscopy, using an HR LabRam800 system equipped with an Olympus BX40 confocal microscope. A Nd:YAG laser beam (532 nm) was focused by a 50X microscope objective onto a spot close to 1 µm diameter of the sample surface. The laser power on the sample (5 mW) was regulated by a neutral density filter to avoid sample heating and structural changes. A CCD camera was used to record the spectra, usually averaged for 100 accumulations in order to improve the signal to noise ratio. All spectra were calibrated using the 521 cm^{-1} line of a silicon wafer, spectra were obtained between 100 and 1200 cm^{-1} with a resolution of 1 cm^{-1}.

2.3.8 Temperature-programmed reduction

The TPR measurements were carried out on a Micromeritics AutoChem II 2920 automated analyzer equipped with a temperature conductivity detector (TCD). Approximately 60 mg of sample was pretreated in situ at 400 ° C for 2 h under airflow in a quartz reactor using a tubular furnace, subsequently the sample was cooled under an Ar flow. The reduction step was carried out under a flow of a mixture Ar / H_2 (90/10 mol / mol and 50 mL / min) and was recorded from environmental temperature to 1000 °C. The outlet gas was monitored on-line with a TCD, converting the obtained signal to concentration units through a calibration curve. The measurement has an experimental error of ±3%

2.3.9 Ammonia thermodesorption

Ammonia TPD experiments were carried out in a vacuum TPD system. Analysis was performed on a Micromeritics AutoChem II 2920 device. 50 mg of a calcined sample was taken and in situ pretreated at 500 ° C for 30 min in a helium flow to remove physisorbed water and other pollutants. Subsequently, sample was cooled to 120 ° C and exposed to a mixture stream of NH_3/He (10:90 mol: mol, flow of 20 mL / min) for 30 min. The desorption of ammonia was carried out in a He gas flow (50 mL / min) of 120 ° C at 500 ° C with a heating rate of 10 ° C / min, keeping the final temperature until the base line was reached. The outlet gas was monitored on-line with a TCD, converting the obtained signal to concentration units through a calibration curve.

2.3.10 Transmission electron microscopy

Sulfided catalysts were dispersed by ultrasound in heptane and the suspension was collected on carbon-coated grids. TEM analysis were carried out using a JEOL 2010 microscope (resolution of 1.9 Å). The micrographs were processed with the Gatan Digital Micrograph software to perform statistics analysis and quantify the slab length and the stacking of the crystallites.

2.4. Catalytic activity tests

The HDS activity tests were performed in a batch reactor at 300 ° C for 8 h and a total pressure of 7.3 MPa, using H_2 to pressurize, the reaction mixture that was a solution of DBT in n-hexadecane (1300 ppm S). Previously, catalysts were activated ex situ (0.15 g, 80–100 Tyler mesh, 0.165 mm of average particle diameter) in a U-shaped glass flow reactor at 400 ° C for 4 h, under a current of 15 % v/v. H_2S/H_2 at atmospheric pressure with a flow of 20 mL / min. After sulfurization, catalysts were transferred in an inert atmosphere (Ar) avoiding contact with air to a three-phase slurry batch reactor (Parr 4562 M). 40 mL of DBT in n-hexadecane solution was used. The operation conditions were carefully chosen to avoid the external and/or internal diffusion limitations, were hydrogen pressure, PH_2 was about 1100 psi, T = 300◦C, working at 300 rpm of mixing speed during 8 h. Aliquots were taken each hour through the reaction time and analyzed in a gas chromatograph Agilent 6890 equipped with a flame ionization detector and Econopac-5 capillary column (Altech).

The obtained products from the main reaction routes as direct desulfurization (DDS) was the biphenyl (BP), and from the hydrogenation (HYD) were the cyclohexylbenzene (CHB) and dicyclohexyl (DCH). The amount of DBT and the amount of these products through reaction time was followed through the gas chromatography analysis, with this data was calculated the conversion percent of DBT. Kinetic constants were determined (k) assuming the pseudo-first order for the DBT concentration and zero-order for the feeding of H_2 in excess. This kinetic constant k [=] h^{-1} was normalized considering the reaction volume and the mass of catalyst employed (k* expressed as L g_{cat}^{-1} s^{-1}). Calculations were made with the integral, initial rate method (eq. 1), also calculations were made using the least squares method for comparison purposes:

$$k = \frac{-ln(CDBT)}{t_r}, \qquad \text{(eq. 1)}$$

3. Results and discussion

3.1 Characterization of supports

From TGA and DSC analysis results, a temperature of 400 ºC for thermal treatment of supports and catalytic precursors was chosen. First, textural properties such as specific surface area, mean pore diameter, pore diameter distribution and total pore volume were determined in the annealed supports. From table 1, it can be seeing that the specific surface area of Al_2O_3-MgO decreases about 10 % and the specific surface area of Al_2O_3-MgO-K_2O decreases about 15 % with regard to the surface area of Al_2O_3 support. Total pore volume decreases almost 15 % in the Al_2O_3-MgO-K_2O support, the observed changes in the textural properties can be attributed to the lower specific surface area of the MgO and to the non-porous structure of K_2O, the mean pore diameter becomes a little bit bigger with MgO and K_2O incorporation. Physisorption isotherms are shown in figure 1, a characteristic type IV is seen attributed to mesoporous materials, and the hysteresis cycle is distinctive of the bottle-neck type pores accordingly to the IUPAC classification as H1-type reported by Leofanti [28]. Elemental chemical composition of the supports, determined from XPS analysis, is shown in table 2, the atomic values agrees well with the expected theorical values.

The X-ray powder diffraction pattern of the alumina support (figure 2.a) shows peaks at 2θ= 37.6, 39.5, 45.8 and 67° corresponding to the γ-Al_2O_3 phase (JCPDF-10-0425). The XRD pattern of the Al_2O_3-MgO support shown in figure 2.b present, additionally to the peaks of the γ-Al_2O_3, two small peaks at 2θ = 42.8 and 62.1° characteristics of the periclase (MgO) crystalline phase (JCPDF 75-0447). Signals corresponding to AlOOH are also observed. The XRD pattern of the Al_2O_3-MgO-K_2O support (figure 2.c) seems to show small peaks at 2θ= 27.6 and 39.5° suggesting the presence of the K_2O crystalline phase (JCPDF-23-0493).

The infrared spectra shown in figure 3, do not display peaks attributed to organic groups, indicative of the complete elimination of formic acid used to prepare the paste of AlOOH. However, some peaks close to 1501, 1406 and 1643 cm^{-1} are observed. These are associated to (COO) of bidentate carbonates, –O-CO_2 vibration in monodentate carbonates and -OH from physisorbed water respectively and are attributed to the CO_2 adsorbed from the environment into the basic sites of the supports. This bands were expected since MgO and K_2O are materials that have basic sites. Supports acidity was determined from the NH_3-TPD measurements. Table 3 shows the total number of acidic sites (TNAS) as a concentration with units of µMol of NH_3 desorbed/g of supports and CoMoW catalysts. It is observed a decrease in the TNAS of 5% for the Al_2O_3-MgO support, whereas a greater decrease of about 50 % for

the Al_2O_3-MgO-K_2O support was observed. The decrease in the acidity is as follows: Al_2O_3 > Al_2O_3-MgO > Al_2O_3-MgO-K_2O.

The total number of acid sites (TNAS) was determined as the area under the TCD signal of NH_3 desorbed. This was done in three temperature intervals: a) 120-200 ºC where NH_3 is desorbed from the weakest acid sites, b) 200-400 ºC where is observed desorption of NH_3 from medium acid sites and c) 400-500 ºC where is assumed that NH_3 is desorbed from stronger acid sites. Acid strength reported in table 3 was determined as the ratio of NH_3 desorbed at 400-500 °C/200-400 ºC. It seems, that acid strength remains almost constant in Al_2O_3 and Al_2O_3-MgO supports, whereas an increase of 26 % in acid strength in Al_2O_3-MgO-K_2O support is observed. From table 3 is observed that MgO addition decreases the concentration of NH_3 thermodesorbed in all temperature intervals, which is associated to a lower number of acid sites than in the Al_2O_3 support. The K_2O incorporation to the support decreases in a greater proportion the concentration associated to the number of acid sites respect to the Al_2O_3 and the Al_2O_3-MgO supports. These decrease in the number of acid sites can also be seen in the figure 4, because the TCD signal is related to the concentration of NH_3-thermodesorbed from acidic sites. Therefore, it is clear that acid sites decrease with the incorporation of MgO and K_2O since these contain some basic sites, acid strength remains in supports when MgO is added, however in Al_2O_3-MgO-K_2O support was observed an increase in its acid strength. The change in this relationship can be associated most probably, to the higher electronegativity of the K^+, that when is incorporated besides the O_2^- promotes an inductive effect and gives them a slight increase in acidity.

3.2 Characterization of catalytic precursors

After supports impregnation with the low acidity solution (CoMoW), some studies were done about the dispersion of these precursors of the active phase, the effect of the catalytic support and mainly the effect of their acidity and acidic strength. Firstly, elemental chemical composition was determined in each catalytic precursor quantified from the corresponding XPS spectrum. Table 4 shows the atomic contents in the catalytic precursors; these results are in good agreement with the expected theoretically. Using the atomic content in table 4 were calculated the atomic ratios in the catalytic surface as follows [Co/(Co+Mo)] = 0.6 and [W/(Co+W)] = 0.3. Textural properties were determined in the catalytic precursors using N_2-physisorption, data is shown in table 5. The main result is a decrease close to 23 % in the specific surface area of the precursors of catalysts to the respective support, which can be considered a result of the decrease in the total pore volume. The total number of acidic sites

(TNAS) were determined using the NH_3-TPD technique. The TNAS decreases in 12 % in catalytic precursors containing MgO and 56 % in that containing MgO-K_2O as is shown in table 3. Also, the acid strength decreases 30 and 13% for the same catalysts.

The addition of the precursors of active phases CoMoW on the supports decrease the TNAS, and comparing the CoMoW/Al_2O_3-MgO-K_2O with the CoMo/Al_2O_3-MgO-K_2O catalyst is observed a decrease in 57.3 % in the TNAS when catalyst contain W, which can be explained as a dilution effect in this case and to the change in the chemical environment of the catalytic formulation, caused by the combined chemical properties such as electronegativity, acid-base properties and polarizability in these materials

It is assumed that the increase in basic sites contained in the MgO and K_2O causes this decrease in the TNAS; the presence of this basic sites is shown in figure 5, from IR spectra of catalytic precursors taken at environmental conditions in the region from 1800 to 1200 cm^{-1}, there are some species of carbonates adsorbed onto the basic sites as carbonates monodentated evidenced by the bands in region 1370-1300cm^{-1}, bidentates with bands in the region from 1620-1530cm^{-1} and also some ionic carbonate 1439 cm^{-1} [30]. Thus, it is clear that whereas basic sites become to appear, TNAS decreases in catalytic precursors. The crystalline structure does not show any important changes respect to the supports as can be seen in figure 6. Again, the main diffraction lines are located at 2θ = 37.6, 39.5, 45.8 and 67° attributed to the γ-Al_2O_3 crystalline phase (JCPDF 10-0425) for all catalytic precursors. Small features at 2θ = 42.8 and 62.1° attributed to the periclase crystalline phase are observed in figure 6 b). The diffraction lines attributed to the K_2O crystalline phase almost disappear. It is worth noting that peaks attributed to the agglomerated MoO_3, WO_3 or Co_3O_4 are absent. This can be explained in terms of the high dispersion of these compounds, or by a dilution effect due to their lower amount as well as by their small crystallite size under the detection limits of the XRD technique. To analyze more deeply the catalytic precursors Raman spectroscopy was used. Figure 7 I) shows the Raman spectra of the catalytic precursors, supported on Al_2O_3, Al_2O_3-MgO and Al_2O_3-MgO-K_2O. The main feature in these spectra is a band close to 950 cm^{-1} with other signals at 680, 521, 480 and 327 cm^{-1}. The bands at 960 and 340 cm^{-1} are attributed to the symmetric stretching and bending mode of the Mo=O bond of octahedrally coordinated polymeric molybdenum oxide species respectively. It is worth mentioning that no evidence of Raman bands attributed to the MoO_3, WO_3 or Co_3O_4 crystalline phases was found suggesting a good dispersion of the CoMoW active phases without agglomeration. As reference figure 7 II) shows the spectra corresponding to these crystalline oxides. It seems that

the bands at 680, 521 and 480 cm^{-1} observed in the catalytic CoMoW precursors can be assigned to the Co_3O_4. In order to gain insight about the kind of surface dispersed species, the band at high frequency was deconvoluted using Gaussian functions. Figures 8 a), b) and c) show the fittings done in each case. The main contributions close to 960 and 925 cm^{-1} are clearly seen. As mentioned before the band at 960 cm^{-1} is assigned to the symmetric stretching mode of the Mo=O bond whereas the band at 925 cm^{-1} could be associated with the Co–Mo interaction species and/or to crystalline $CoMoO_4$. Two changes in these bands reveal the effect of the used support on the dispersed catalyst. First, a shift of the most intense band from 963 (Al_2O_3 support) to 958 cm^{-1} (Al_2O_3-MgO and Al_2O_3-MgO-K_2O) suggesting that the Mo species changes from a polymolybdate phase ($[Mo_8O_{26}]^{-2}$) to adsorbed monomeric species (Co–Mo interaction, Mo−O in MoO_4^{2-}); second, a clear change in their relative intensities suggest a higher proportion of $[Mo_8O_{26}]^{-2}$ species in the catalytic precursor supported on Al_2O_3, which changes with acidity in support, becoming a higher proportion of the WO_4^{2-} specie in the Al_2O_3-MgO and Al_2O_3-MgO-K_2O supports. Table 6 resumes the Raman bands fitted with the corresponding anionic species and kind of coordination. This fact was analyzed and complemented through the UV-Vis DRS spectra obtained in the diffuse reflectance mode shown in figure 9. These spectra show some features at 215, 268, 300 nm due to Mo^{6+}species, and at 541, 587 and 641 nm due to Co^{2+}species. From figure 9 the ratio of bands Mo[O]/Mo[T] bands located at 300 nm attributed to the Mo[O] and at 268 nm assigned to the Mo[T] increases its intensity in catalytic precursors supported on Al_2O_3-MgO and Al_2O_3-MgO-K_2O, which is attributed to the agglomeration of the molybdenum species as was reported [31]. Furthermore, spectra show three bands located at 541, 587 and 641 nm, this controversial bands can be attributed accordingly to Vakros et al and Hanke et al [31-32] to Co^{2+} in tetrahedral coordination. Matralis et al [33] relate this band with some $CoAl_2O_4$ in catalytic surface. It is observed that the K_2O addition has two main effects, by one-hand causes an increase in the 641 nm band and on the other hand increase intensity of 300-500 nm bands.

Accordingly, to the reported before by Weber [29], these UV-Vis DRS spectra were processed, their bandgap energy was calculated, which is empirically related to the particle agglomeration. Band gap energy was calculated from the Tauc method, using the Kubelka-Munk equation, assuming samples are semiconductors with an indirect allowed electronic transitions. For this family of catalytic precursors, there is a large range of edge energies, even when this have a very low metallic loadings. In this case, in figure 10 the absorption edges are to span 1.15 eV range with the larger aggregates having smaller energies in 2.17 eV, this

results were correlated with the shift towards lower band gap energies, that accompany the growth of semiconductor particles as Weber report in 1995, in the study of isopolymolybdate families, [29]. From figure 10, can be concluded that catalytic precursors supported in samples containing K_2O and MgO have high agglomeration of the polytungstates and isopolymolybdates species as in the CoMoW masic catalyst, and there is a higher dispersion of this species on the Al_2O_3 support. The importance of analyze dispersion of the polytungstates and isopolymolybdates species is related to the reducibility of the precursors of the active species, and this is related with the easily for be sulphurated; finally, the sulfurs of molybdenum and also the tungsten contain the active sites in their crystallite defects, which are the sulfur vacancies. By the aforementioned, was important to determine the reducibility degree in catalytic precursors by the TPR technique, from thermograms shown in figure 11, can be seen that polymolybdates and polytungstates are easier to reduce when they are supported on Al_2O_3 and Al_2O_3-MgO (figure 11 a) and b), there are signals of reduction at temperatures as low as 423 ^oC. Catalytic precursor supported on Al_2O_3-MgO-K_2O show signals of reduction at higher temperatures than the observed in the reduction of the conventional formulation CoMoW/Al_2O_3. From the aforementioned, it is expected a better sulfidation of active phases supported on Al_2O_3 than the observed on the Al_2O_3-MgO-K_2O support.

3.3 Characterization of catalysts

To analyze sulfidation degree of the MoS_2 and WS_2 active phases transmission electron microscopy (TEM) on sulfided catalysts was performed. From figure 12 a-c, were counted statistically the stacking slab and also slab length in micrographs for each catalyst, the statistics are accordingly with the expected from TPR thermograms, there are a small population of slabs in catalysts supported on Al_2O_3-MgO-K_2O. Statistic slab length of active phases was shown in figure 13 a) and their stacking number in figure 13 b). The main slab length of MoS_2 and WS_2 is between 21-40 Å, followed by the 41-60 Å, in this case always the active phases supported on the Al_2O_3-MgO-K_2O predominate. From figure 13 b) is observed a stacking of one slab mainly in active phases supported on Al_2O_3, whereas in the Al_2O_3-MgO-K_2O support can be seen the stacking of 2, 3 and also 4 slabs. This stacking in the formulation containing K_2O gives information on MoS_2 and WS_2 with active sites non-accessible, this lesser accessibility to the catalytically active sites will probably be a reason for decrease catalytic activity promoted by this sulfur vacancies. It is expected that the catalytic

formulation with less stacking and greater dispersion of the active phases will have the catalytic active sites (sulfur vacancies) completely accessible and this will enhance catalytic activity.

3.4 Catalytic performance of CoMoW Catalysts

Catalytic activity in HDS of DBT reaction was evaluated for each catalytic formulation. DBT conversion percent from reactions through reaction time is shown in table 7, conversions of 91 and 86 % where obtained after 8 h of reaction time, for catalytic formulations supported on Al_2O_3 and Al_2O_3- MgO. The catalytic formulation containing K_2O reach 55 % of DBT conversion at the same time of 8 hours, which is the lowest conversion obtained and represents a decrease of 40% in conversion percent respect to the conventional formulation. Decrease in the DBT conversion percent reached in this CoMoW/Al_2O_3-MgO-K_2O catalyst is explained in terms of the agglomeration of the MoS_2 and WS_2 active phases as was seen from the slab length and stacking slabs of 2, 3 and 4 as can be seen in figure 12 c) of TEM. Figure 14 a) shows the DBT conversion percent reached through reaction time for each catalytic formulation. Table 7 shows the kinetic constants for the initial reaction rates obtained with the integral method assuming a pseudo first-order from the slope in graphics of Ln (C/Co) versus time reaction; for comparison purposes kinetic constants rates were also determined using the least squares method, both values of kinetic constants are shown in the same table 7 with a good correlation between them and shown good correlation as well with the DBT conversion percent. The selectivity analysis of catalytic formulations, given by the DDS/HYD ratio (table 7), was 4.4 and 5.1 for catalysts supported on Al_2O_3 and Al_2O_3-MgO respectively. Although CoMoW/Al_2O_3-MgO-K_2O catalyst reached the lowest DBT conversion percent (55%) this catalytic formulation shows the highest selectivity towards direct desulphurization (DDS) with the highest DDS/HYD ratio of 7.3, as can be seen in figure 15. This can be explained in terms of the bifunctionality of the catalytic formulation, acidic sites and sulfur vacancies, in other words in the CoMoW/Al_2O_3-MgO-K_2O acidity is decreased in a greater proportion, whereas basic sites become to appear; the decrease in acidity changes active phase dispersion, agglomerating the active phases or the accessible active sites (sulfur vacancies), agglomeration also decreases the sulfurization degree, which is directly related to the decrease in DBT conversion. This stacking number and slab length are also directly related with the support and molybdenum charge, defining the preferred reaction route through DDS or HYD.

4. Conclusions

A novel catalytic formulation CoMoW supported on γ-Al_2O_3 modified with MgO and K_2O was obtained. Its low acidity enhanced the catalytic activity in the HDS of DBT towards direct desulfurization. It was found that addition of magnesium and potassium to the catalytic support decreases the number of acid sites. The reduced number of acidic sites and controlled acidity strength decrease the hydrogenation function increasing its selectivity toward BF products. Clearly the change in the chemical nature of the support, modifying its acidity or basicity, promotes important changes in the dispersion and agglomeration of the precursors of the active species deposited on it. The results of Raman spectroscopy, UV-Vis DRS spectroscopy and the programmed temperature reduction show that the incorporation of magnesium and especially with the incorporation of both magnesium and potassium in the support precursors of the active phases causes agglomeration. This affects the sulfidation degree, promoting agglomeration in active phases, which could be the responsible of the low sulfidation and that active sites (sulfur vacancies) not be catalytically accessible; in agreement with the results obtained in the samples sulphurated by TEM, it was observed an increase in the stacking of the crystalline planes in 2-4 slabs, as well as slab lengths between 20-60 Å. It is concluded that the acidic sites and also the basic sites are the main responsible of the decrease of the hydrogenating function and to the increase in selectivity towards direct desulfurization in the catalytic formulations.

Acknowledgements

D.A. Solís-Casados thanks the UAEM-4488 project for the financial support granted for the maintenance of the CHEMBET 3000 equipment. C.E. Rodriguez-Nava thanks to CONACyT for the 631531 fellowship. Authors thank to LIA Citlalit Martínez Soto, Dr. Uvaldo Hernández Balderas, Dra. Melina Tapia Tapia, M. en C. Ma. de las Nieves Zavala Segovia, M. en C. Lizbeth Triana Cruz and M. en C. Alejandra Núñez Pineda for technical assistance in CCIQS UAEM-UNAM. Authors also thank to Ivan Puente Lee (USAI) for the HRTEM of sulfided samples.

References

[1] P. Castillo-Villalón, J. Ramírez, R. Cuevas, P. Vázquez, R. Castañeda, *Catal Today* 259 (2015) 140–149

[2] P. A. Nikulshin , A. V. Mozhaev, A. A. Pimerzin, V. V. Konovalov, A. A. Pimerzin. *Fuel* 100 (2012) 24–33

[3] F.J. Méndez, O. E. Franco-López, X. Bokhimi, D. A. Solís-Casados, L. Escobar-Alarcón, T. E. Klimova. *Appl Catal B: Environmental*. 219, (2017), 479-491

[4] M. Absi-Halabi, A. Stanislaus, K. Al-Dolama. *Fuel* 77-7 (1998), 787-790.

[5] T. Klimova, D. Solís-Casados, J. Ramírez. *Catal Today*, 43, (1998), 135-146

[6] J. Grimblot. *Catal Today*, 41(1998) 111-128.

[7] S. L. Amaya, G. Alonso-Núñez, T.A. Zepeda, S. Fuentes, A. Echavarría. *Appl Catal B*: *Environmental*, 148–149, (2014), 221–230,

[8] T. Klicpera, M. Zdrazil. *J of Catal* 206, (2002) 314–320

[9] Song, Chunshan. *Catal Today* 86 (2003), 211–263,

[10] Y. E. Liceaa, R. Grau-Crespo, L. A. Palacio, A. C. Faro Jr. *Catal Today* 292 (2017) 84–96

[11] S. Arias, Y. E. Licea, D. Soares, J. Guillaume Eon, L. A. Palacio, Arnaldo C. Faro Jr.a. *Catal Today* 296 (2017) 187–196

[12] V. Vanrysselberghe, G. F. Froment. *Ind. Eng. Chem. Res*., 35, (1996) 3311-3318

[13] A. L. Barbosa, A. F. Vega, E. de Rio Amador. *Avances en Ciencias e Ingeniería*, 5(3), (2014), 37-60

[14] D. Valencia, I. García-Cruz, T. Klimova. *Stud in Surf Sci and Catal* 175 (2010), 529-532

[15] I.V. Babich, J.A. Moulijn. *Fuel*, 82 (2003) 607–631

[16] I. Mochida, K. Choi. *Journal of the Japan Petroleum Institute*, 47 (3), (2004) 145-163

[17] D. Solís, J. Ramírez, R. Cuevas, R. Contreras, T. Cortéz, M. Aguilar. *Superficies y Vacío*, 20(4), (2007), 19-26

[18] L. Wang, Y. Zhang, Y. Zhang, P. Liu, H. Han, M. Yang, Z. Jiang, C. Li. *Appl Catal A: General* 394 (2011) 18–24

[19] R. Huirache-Acuña, M.G. Sánchez-Bautista, J. Lemus-Ruiz, C. Ornelas, F. Paraguay-Delgado y E.M. Rivera-Muñoz. *Revista Mexicana de Ingeniería Química*. 9 (2) (2010) 209-218

[20] S. Badoga, A. Ganesana, A. K. Dalaia, S. Chand. *Catal Today* 291, (2017) 160-171.

[21] W. L.S. Faria, C.A.C. Perez, D. V. César, L. C. Dieguez, M. Schmal. *Applied Catalysis B: Environmental* 92 (2009) 217–224

[22] S. Badoga, A. Ganesan, A. Dalai, S. Chand, *Catal Today* **291** (2016) 160-171.

[23] B. Caloch, M. S. Rana, J. Ancheyta. *Catal Today*, vol. 98, p. 91–98, 2004.

[24] D. Solís-Casados, L. Escobar-Alarcón, T. Klimova, J. Escobar-Aguilar, S. Romero, C. Morales-Ramírez. *Fuel* 110 (2013) 278–285.

[25] D. Solís-Casados, L. Escobar-Alarcón, T. Klimova, J. Escobar-Aguilar, E. Rodríguez-Castellón, J. A. Cecilia, C. Morales-Ramírez, *Catal. Today* 271 (2016) 35-44.

[26] J. Mendoza-Nieto, O. Vera-Vallejo, L. Escobar-Alarcón, D. Solís-Casados, T. Klimova, *Fuel* 110 (2013) 268-277.

[27] A. V. Pashigreva, O. V. Klimov, G. A. Bukhtiyarova, M. A. Fedotov, D. I. Kochubey, Yu. A. Chesalov, V. I. Zaikovskii, I. P. Prosvirin, A. S. Noskov. *Stud in Surf Sci and Catal* 175 (2010) 109-116

[28] G. Leofanti, M. Padovan, G. Tozzola, B. Venturelli. *Catal Today* 41(1998) 207-219.

[29] S. Weber. *J Catal* 151 (1995) 470-474.

[30] H. Hattori. *Chem. Rev*. 95 (1995) 537-550

[31] J. Vakros, A. Lycourghiotis, G. Voyiatzis. *Applied Catalysis B: Environmental* 96(2010) 496–507.

[32] W. Hanke, R. Bienert, H. Jerchkewitz, Z. Anorg. Allg. *Chem.* 414 (1975) 109.

[33] H. Matralis, Ch. Papadopoulou, A. Lycourghiotis, *Appl Catal A: Gen*. 116 (1994) 221

Figure 1. N_2-Physisorption isotherms of the different supports. a) Al_2O_3, b) Al_2O_3-MgO and c) Al_2O_3-MgO-K_2O

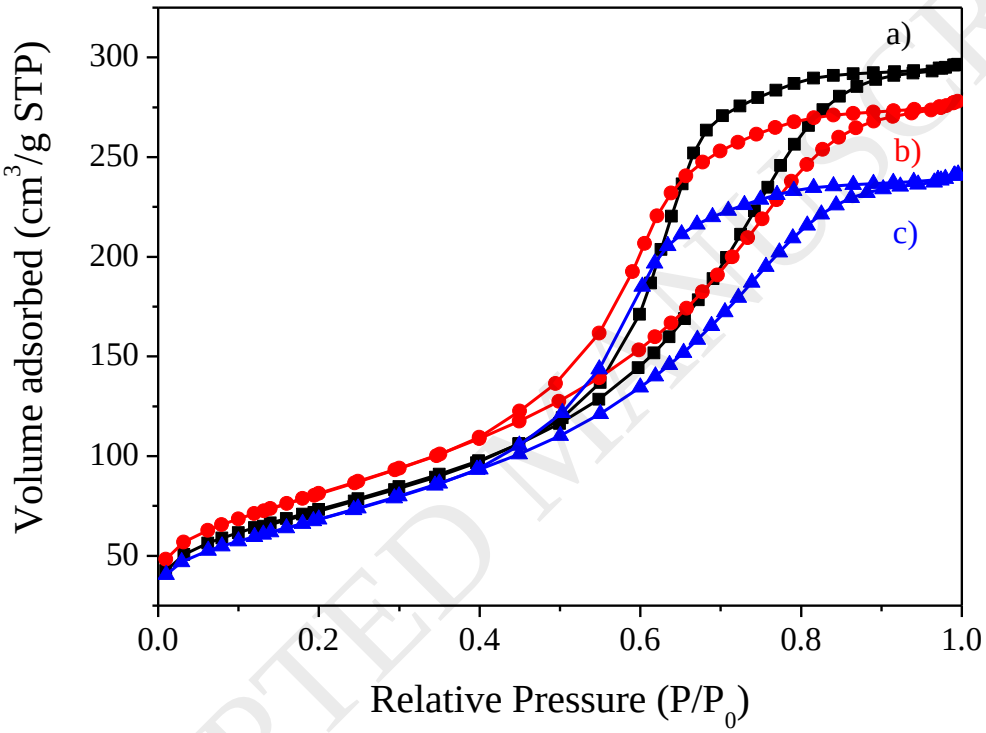

Figure 2. X-ray diffraction patterns of the different supports. a) Al_2O_3, b) Al_2O_3-MgO and c) Al_2O_3-MgO-K_2O

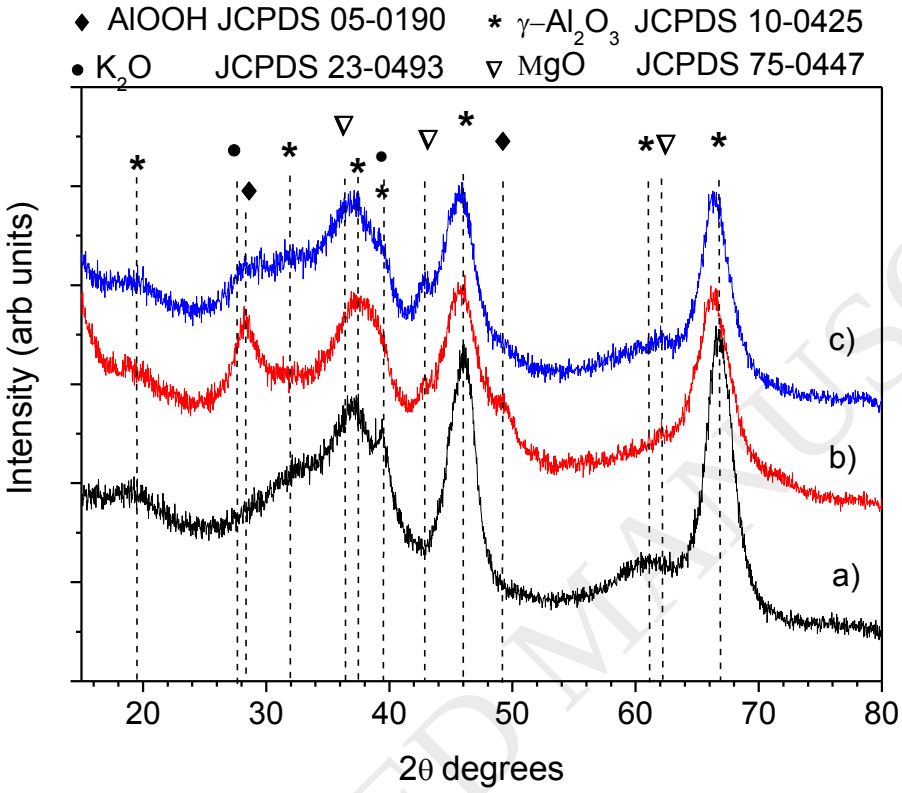

Figure 3. Infrared spectra of the supports. a) Al_2O_3, b) Al_2O_3-MgO and c) Al_2O_3-MgO-K_2O

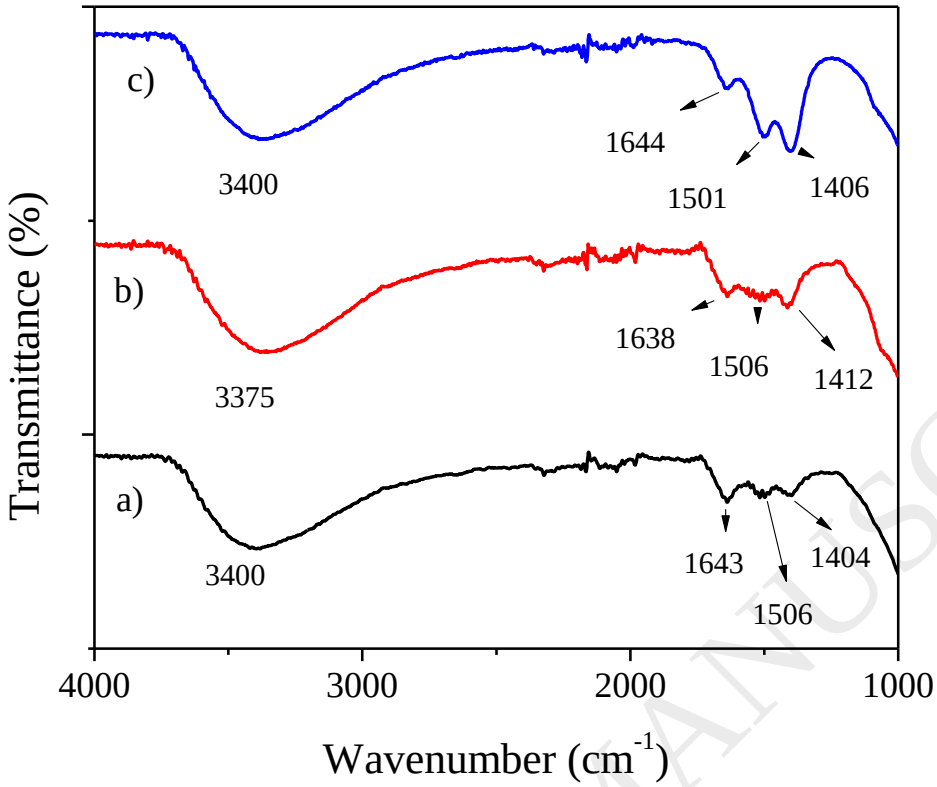

Figure 4. NH_3-TPD of the supports. a) Al_2O_3, b) Al_2O_3-MgO and c) Al_2O_3-MgO-K_2O

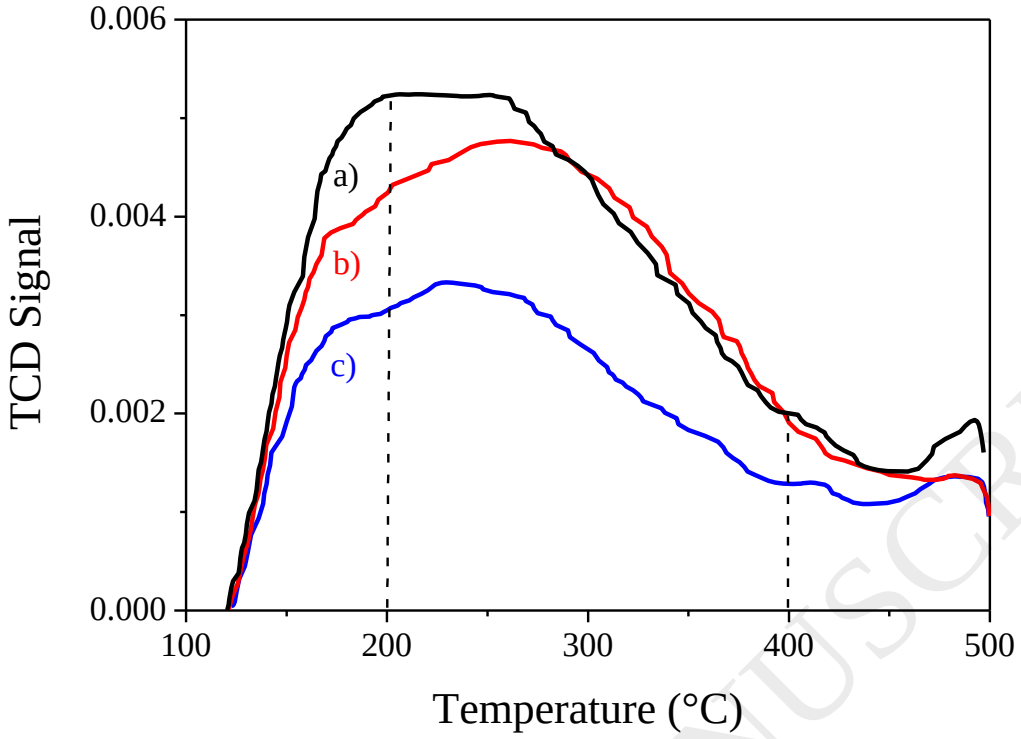

Figure 5. Infrared spectra of the catalytic precursors CoMoW supported on a) Al_2O_3, b) Al_2O_3-MgO and c) Al_2O_3-MgO-K_2O

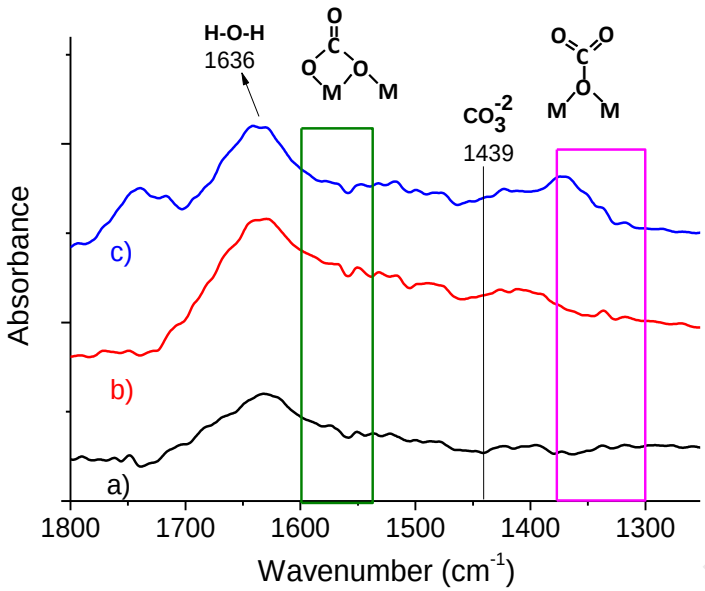

Carbonates	
Ionic	1439 cm^{-1}
Monodentate	1370–1300 cm^{-1}
Bidentate	1620-1530 cm^{-1}

Figure 6. X-ray diffraction patterns of catalytic precursors CoMoW supported on a) Al_2O_3, b) Al_2O_3-MgO and c) Al_2O_3-MgO-K_2O

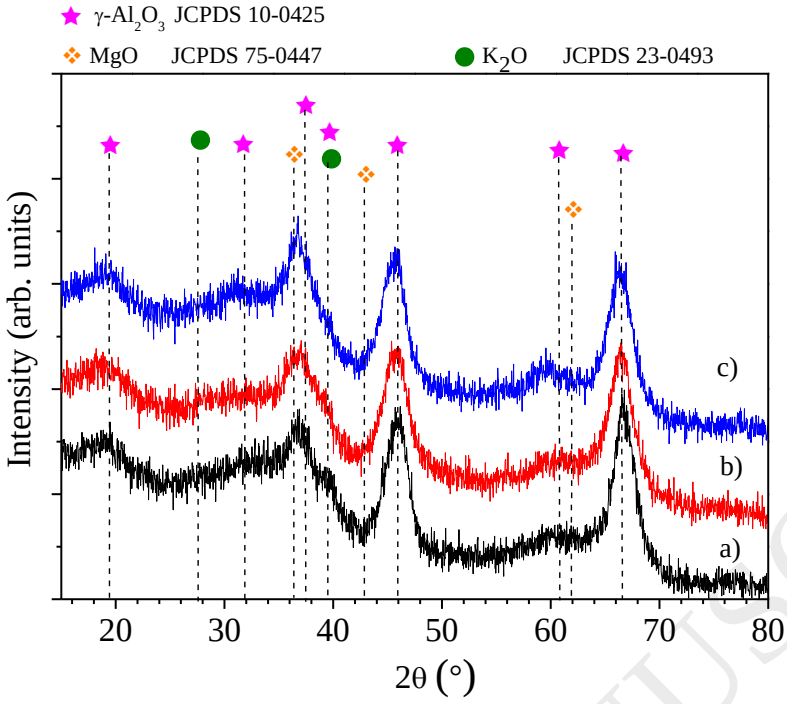

Figure 7. Raman spectra of I) catalytic precursors supported on a) Al_2O_3, b) Al_2O_3-MgO and c) Al_2O_3-MgO-K_2O; and II) agglomerated crystalline phases

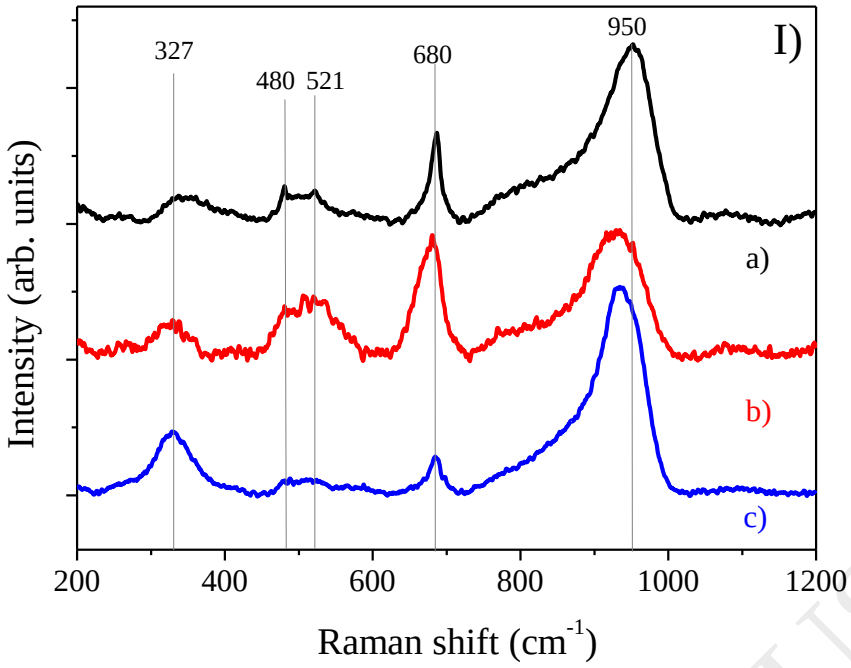

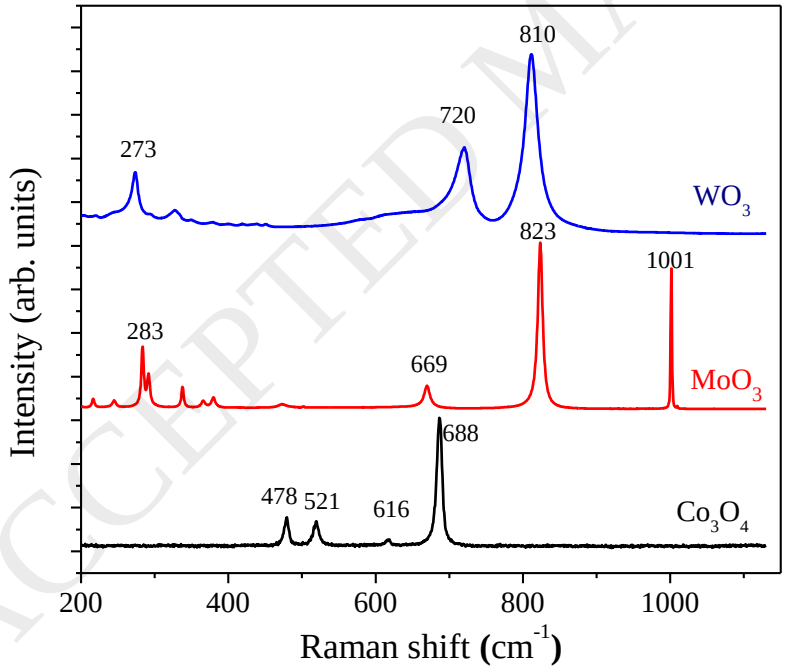

Figure 8. Deconvolution of the Raman band located at 950 cm^{-1} of the CoMoW catalytic precursors supported on a) Al_2O_3, b) Al_2O_3-MgO and c) Al_2O_3-MgO-K_2O

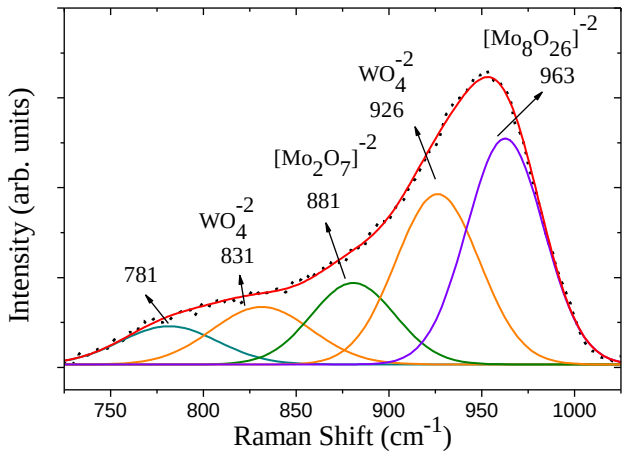

a)

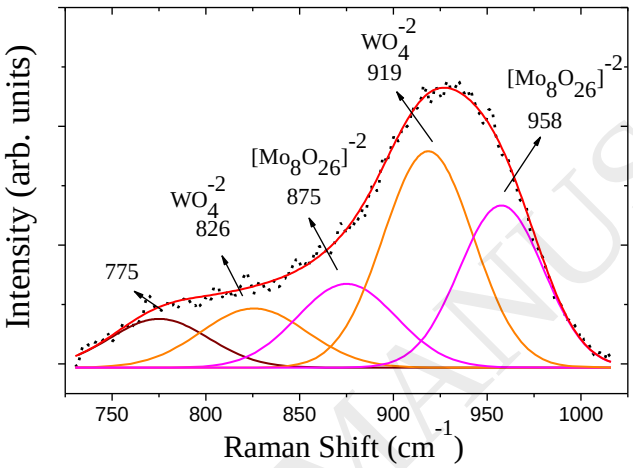

b)

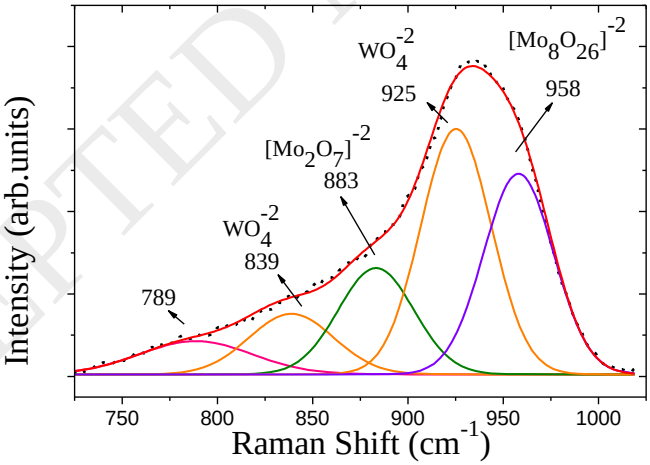

c)

Figure 9. DRS spectra of the CoMoW catalytic precursors supported on a) Al_2O_3, b) Al_2O_3-MgO and c)Al_2O_3-MgO-K_2O

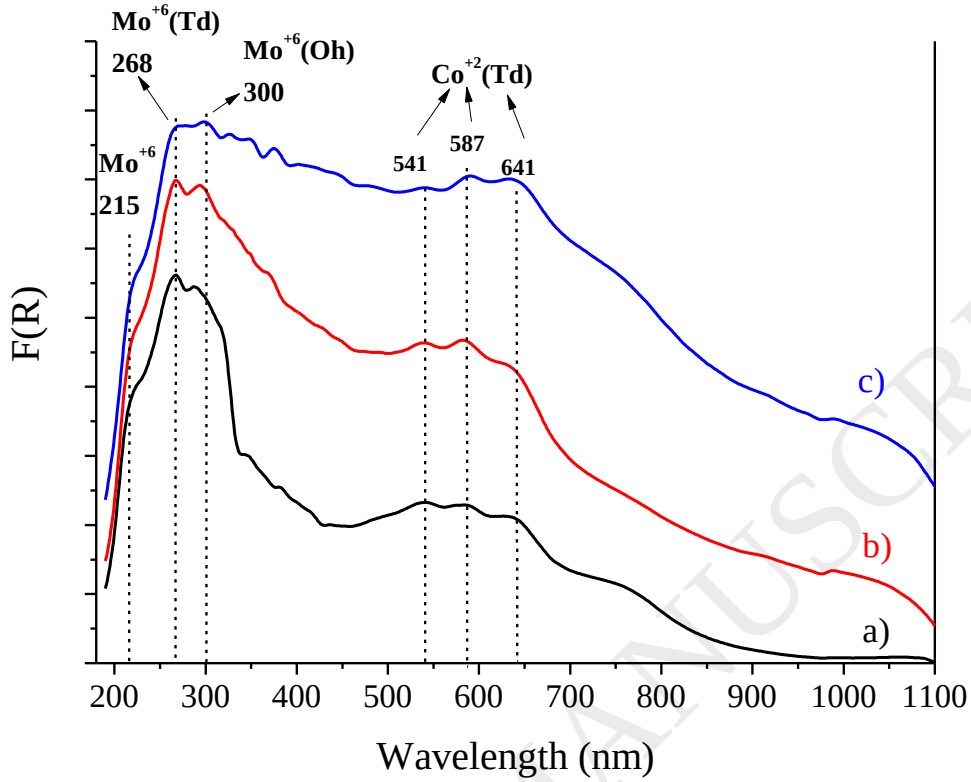

Figure 10. Tauc plots for determination of the optical band gap of the CoMoW catalytic precursors

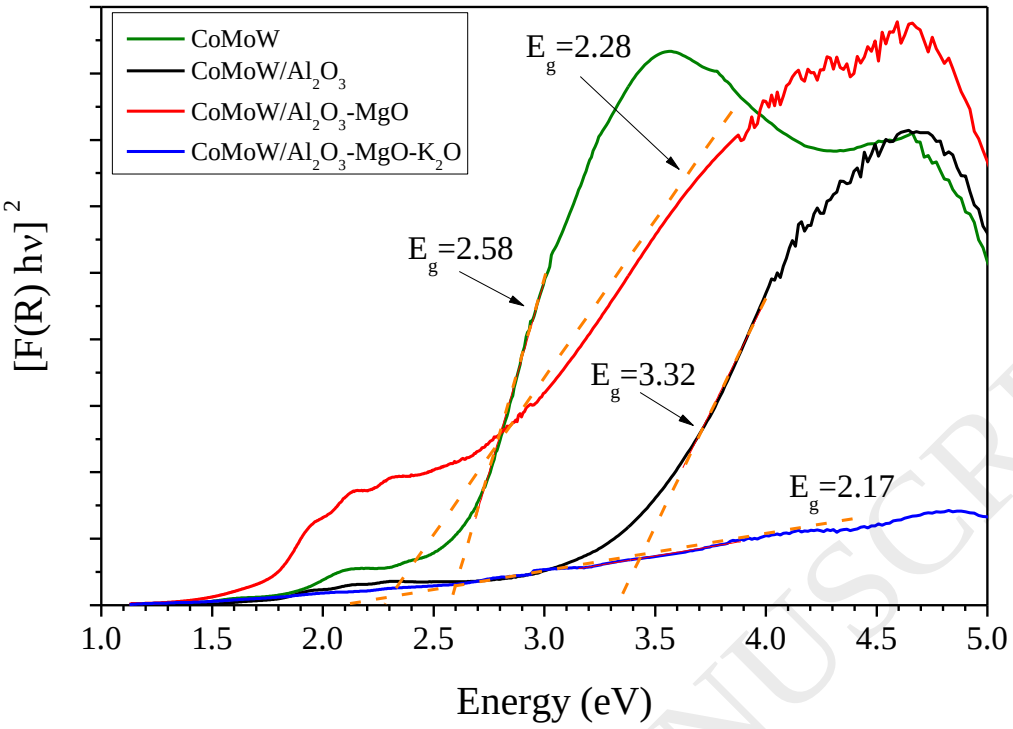

Figure 11. TPR thermograms for CoMoW catalytic precursors supported on a) Al_2O_3, b) Al_2O_3-MgO and c) Al_2O_3-MgO-K_2O

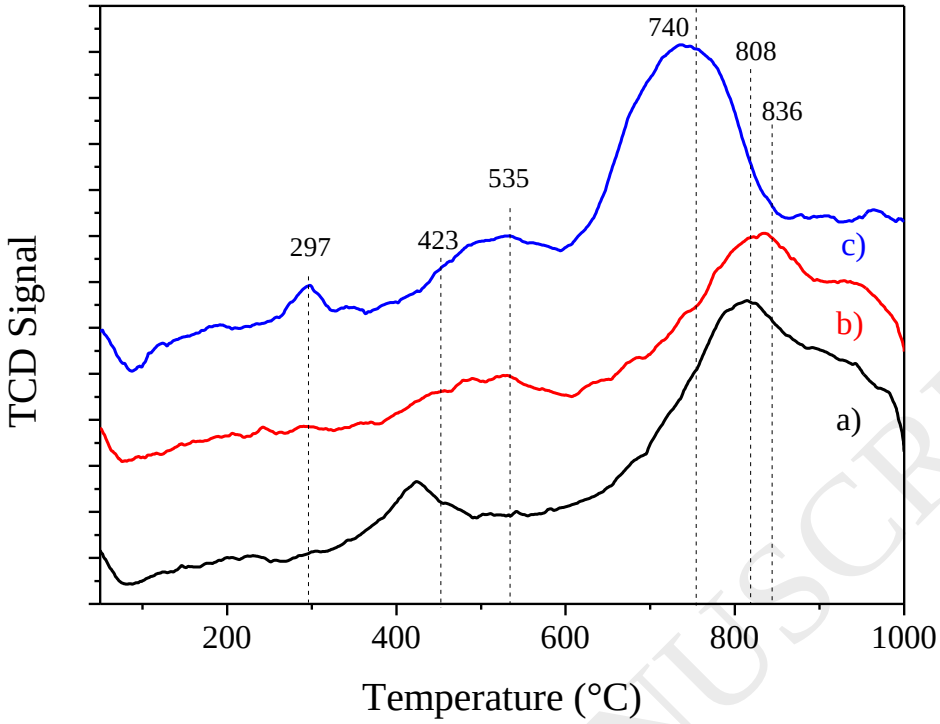

Figure 12. TEM images of CoMoW catalyst supported on a) Al_2O_3, b) Al_2O_3-MgO and c) Al_2O_3-MgO-K_2O

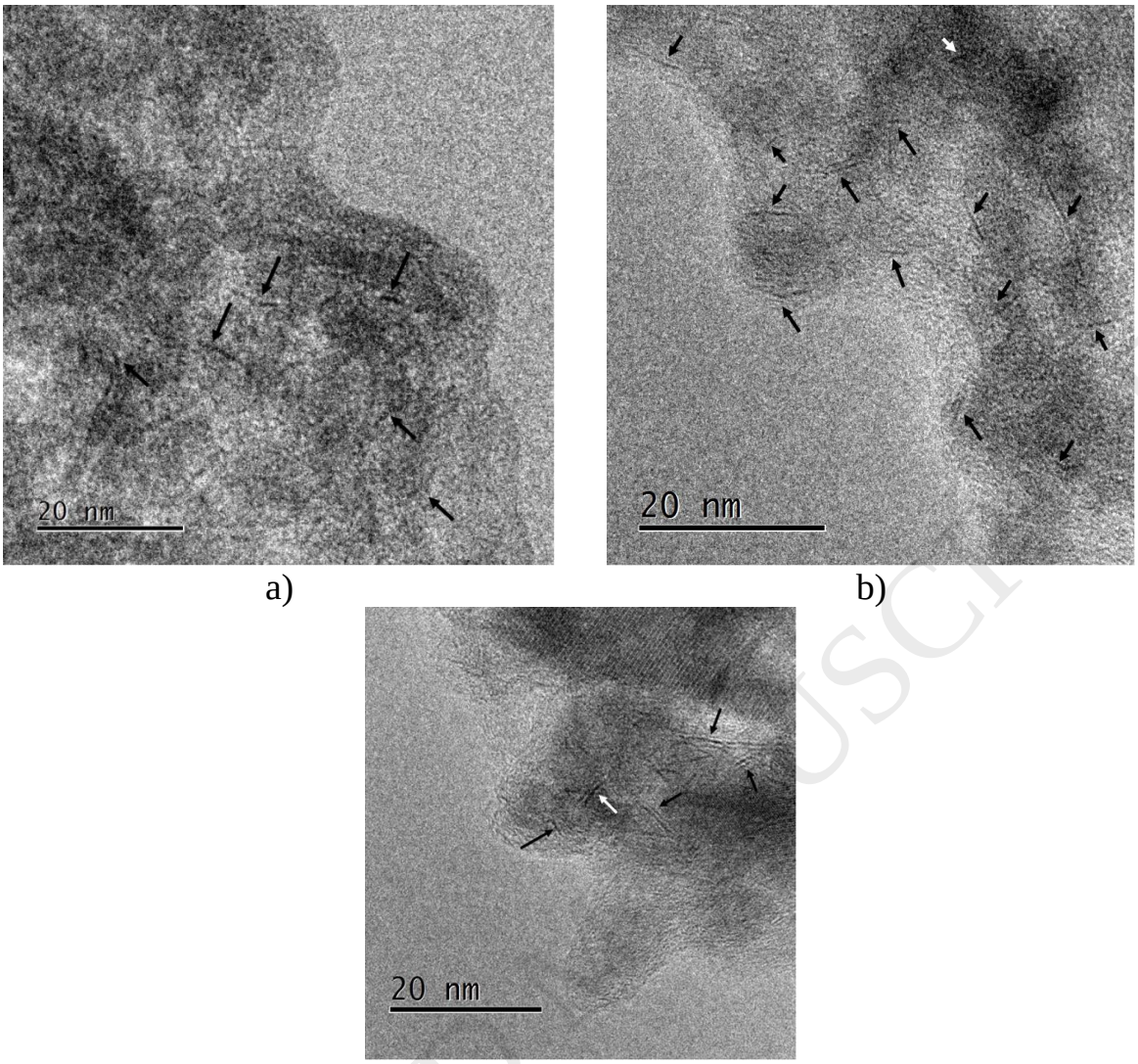

Figure 13. a) Slab length distribution and b) stacking number distribution of WS_2 and MoS_2 crystallites

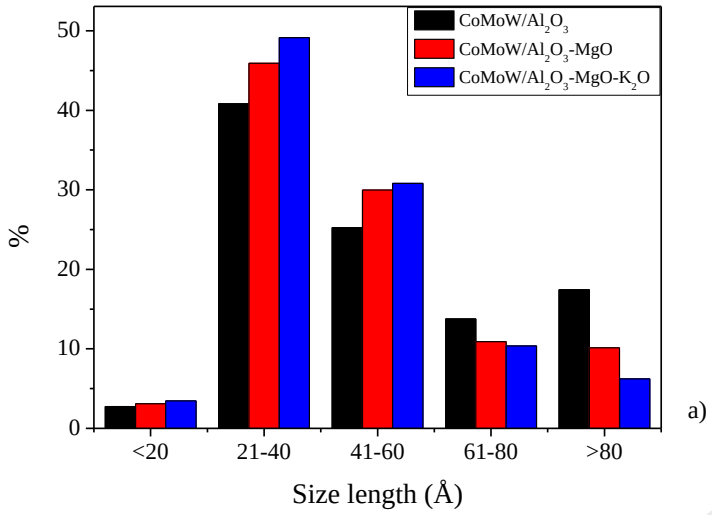

a)

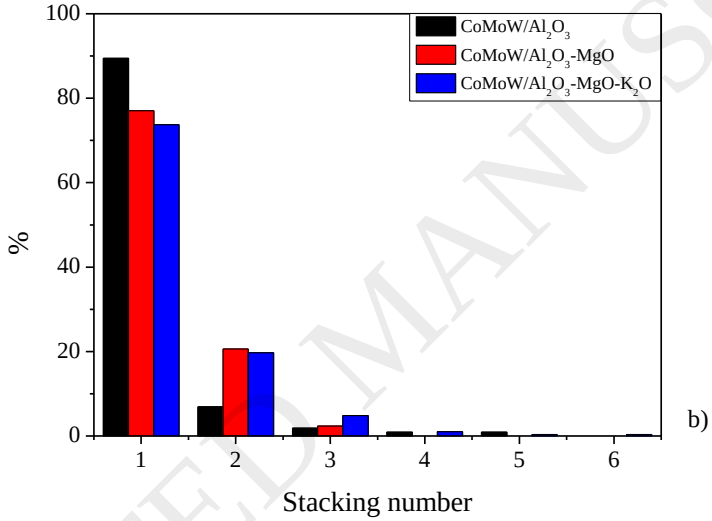

b)

Figure 14. a) DBT conversion as a function of the reaction time, b) Selectivity (DDS/HYD) as a function of DBT conversion percent

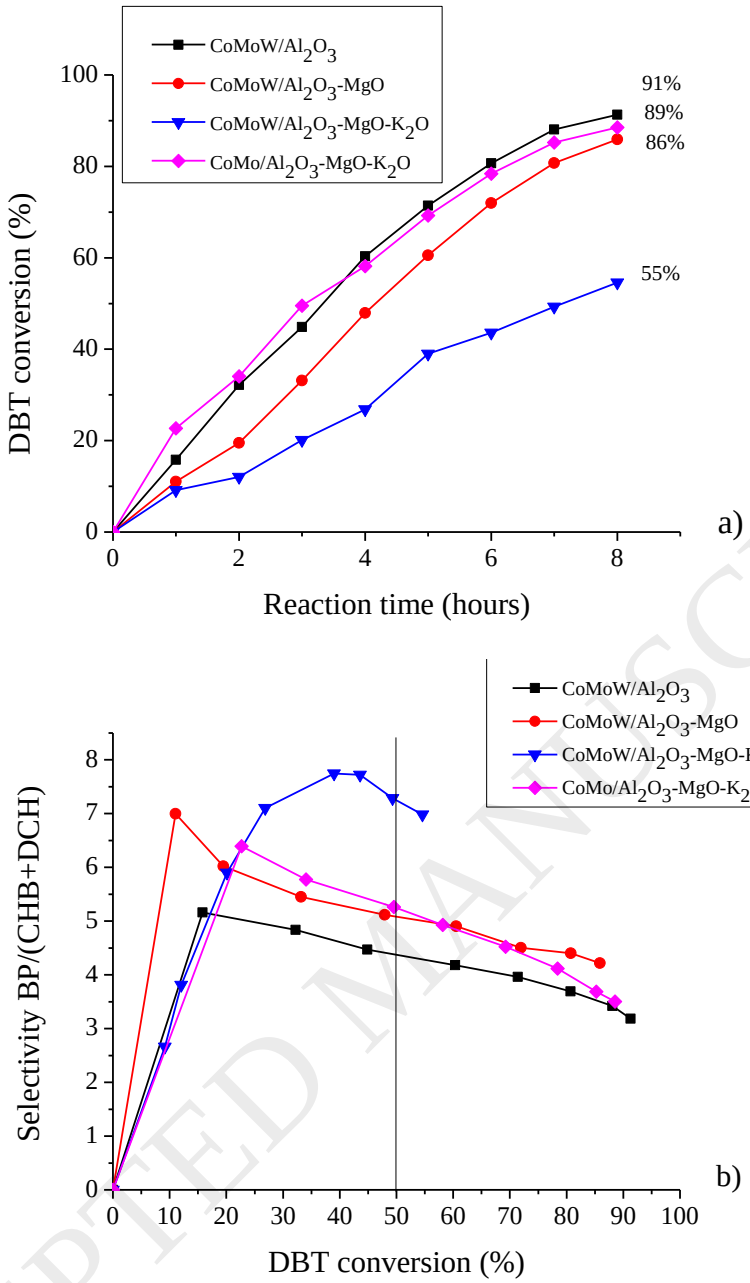

Figure 15. DBT conversion at 8h of reaction time and Selectivity (DDS/HYD) for each catalytic formulation

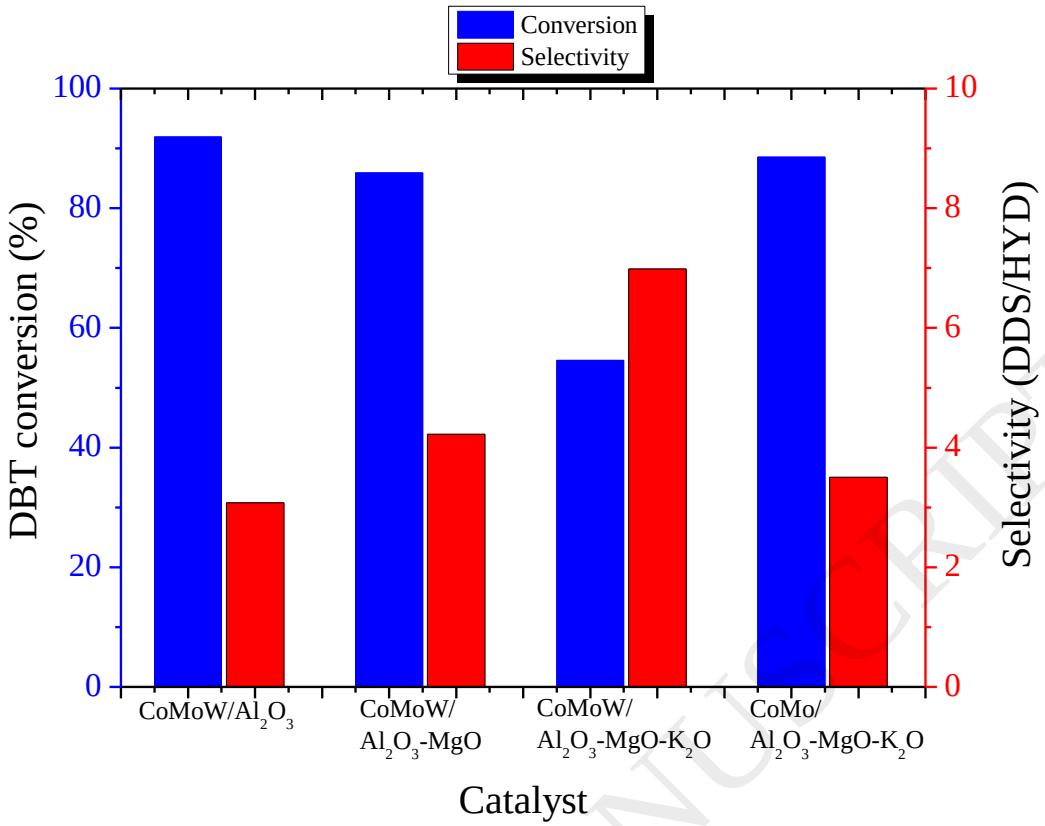

Table 1. Textural properties of supports, Specific surface area, mean pore diameter, and total pore volume

Support	Specific surface area (m^2/g)	Mean pore diameter D_p (Å)	Pore Volume (cm^3/g)
Al_2O_3	294	58	0.42
Al_2O_3-MgO	265	69	0.45
Al_2O_3-MgO-K_2O	250	59	0.36

Table 2. Elemental chemical composition of supports and precursors of catalysts obtained by XPS

	Atomic Content (at %)					
	Supports			CoMoW supported on		
Element	Al_2O_3	Al_2O_3-MgO	Al_2O_3-MgO-K_2O	Al_2O_3	Al_2O_3-MgO	Al_2O_3-MgO-K_2O
O	53	75	77	83	71	76
Al	47	10	11	13	13	9
Mg	-	15	11	-	14	11
K			1		-	2
Co				2	1	1
Mo				1	1	1
W				1	0.5	0.5

Table 3. Acidic sites number and their acid strength

Support	NH_3 desorbed (μmol/g)				
	120-200 °C weak	**200-400 °C medium**	**400-500 °C strong**	**TNAS**	**Acid Strength strong/medium**
Al_2O_3	168	411	92	672	0.22
Al_2O_3-MgO	144	407	88	639	0.22
Al_2O_3-MgO-K_2O	110	260	77	446	0.29
CoMoW/Al_2O_3	168	309	46	522	0.15
CoMoW/ Al_2O_3-MgO	155	275	27	456	0.10
CoMoW/Al_2O_3-MgO-K_2O	85	126	16	228	0.13
CoMo/ Al_2O_3-MgO-K_2O	192	310	32	534	0.10

Table 4. Atomic ratios in catalytic precursors

Catalyst	$\frac{Co}{Co+Mo}$	$\frac{W}{Co+W}$	$\frac{Co}{Co+W}$	$\frac{Co}{Co+Mo+W}$
CoMoW/ Al_2O_3	0.66	0.33	0.66	0.50
CoMoW/ Al_2O_3-MgO	0.50	0.33	0.66	0.40
CoMoW/ Al_2O_3-MgO-K_2O	0.50	0.33	0.66	0.40
CoMo/ Al_2O_3-MgO-K_2O	0.36	-	1.0	0.36

Table 5. Textural properties of supported catalysts, Specific surface area, mean pore diameter, and total pore

CoMoW supported on	**Area (m^2/g)**	**D_p (Å)**	**Volume (cm^3/g)**
Al_2O_3	225	66	0.4
Al_2O_3-MgO	210	61	0.3
Al_2O_3-MgO-K_2O	196	57	0.3

Table 6. Raman bands

Anionic specie	Raman shift	Coordination
$[Mo_2O_7]^{-2}$	353, 883 cm^{-1}	Octahedral
$[Mo_8O_{26}]^{-2}$	365,958 cm^{-1}	Octahedral
WO_4^{-2}	327, 839, 925 cm^{-1}	Tetrahedral
Co_3O_4	480, 521, 680 cm^{-1}	

Table 7. DBT conversion at 4 and 8 h of reaction time, kinetic constants and selectivity

CoMoW supported on	**DBT Conversion (%)**		***k* (initial rate)**	***k**** **(initial rate)**	***k**** **(least squares)**	**Selectivity at conversion 50%**	
	4 h	**8 h**	h^{-1}	**L $g_{cat}^{-1}s^{-1}$**	**L $g_{cat}^{-1}s^{-1}$**	DDS/HYD	HYD/DDS
Al_2O_3	60	91	0.215	1.52E-05	1.71 E-05	4.4	0.23
Al_2O_3-MgO	48	86	0.145	1.03 E-05	1.30 E-05	5.1	0.20
Al_2O_3-MgO-K_2O	27	55	0.076	5.54 E-06	6.70 E-06	7.3	0.14
CoMo/Al_2O_3-MgO-K_2O	58	89	0.221	1.62 E-05	1.75 E-05	5.3	0.19

*k** is expressed as L g_{cat}^{-1} s^{-1}